Morphological and electrical properties of $SrTiO_3/TiO_2/SrTiO_3$ sandwich structures prepared by plasma sputtering*

Saqib Jabbar[1,2,†], Riaz Ahmad[1], and Paul K Chu[2,†]

[1] *Government College University, Lahore 54000, Pakistan*

[2] *Department of Physics and Materials Science, City University of Hong Kong, Kowloon, Hong Kong, China*

(Received 5 September 2016; revised manuscript received 26 October 2016; published online 10 December 2016)

$SrTiO_3$ (STO) and TiO_2 are insulating materials with large dielectric constants and opposite signs of the quadratic coefficient of voltage (α). Insertion of a TiO_2 thin film between STO layers increases the linearity of the capacitance in response to an applied voltage, to meet the increasing demand of large-capacitance-density dynamic random access memory capacitors. Both STO and TiO_2 suffer from the problem of high leakage current owing to their almost equivalent and low bandgap energies. To overcome this, the thickness of the thin TiO_2 film sandwiched between the STO films was varied. A magnetron sputtering system equipped with radio frequency and direct current power supply was employed for depositing the thin films. TiN was deposited as the top and bottom metal electrodes to form a metal–insulator metal (MIM) structure, which exhibited a very large linear capacitance density of 21 fF/um^2 that decreased by increasing the thickness of the TiO_2 film. The leakage current decreased with an increase in the thickness of TiO_2, and for a 27-nm-thick film, the measured leakage current was 2.0×10^{-10} A. X-ray diffraction and Raman spectroscopy revealed that TiN, STO, and TiO_2 films are crystalline and TiO_2 has a dominant anatese phase structure.

Keywords: strontium titanate, Raman spectroscopy, plasma deposition, MIM capacitor

PACS: 07.30.Kf, 52.77.Dq, 74.25.nd, 73.61.Ng **DOI:** 10.1088/1674-1056/26/1/010702

1. Introduction

Strontium titanate (STO) thin films are promising for dynamic random access memory (DRAM) capacitors, owing to their high dielectric constant (κ) of ~150 or higher in the crystalline phase,[1] good thermal stability, good durability, and good compatibility with the device fabrication processes.[2,3] In DRAM applications, a flat dependence of the capacitance on the applied voltage is required, but most of the existing high-κ materials exhibit a quadratic voltage dependence $[C(V) - C_o]/C_o = \alpha^2 + \beta$, where C_o is the capacitance at 0 V and α and β are the quadratic and linear coefficients, respectively. For most high-κ materials, α is in the 100–1000 ppm/V^2 range[4–6] and can be reduced in a bilayer capacitor with materials having opposite-sign (positive and negative) values of α.[7] STO has a negative α and can be used in combination with HfO_2, ZrO_2, Al_2O_3, and TiO_2, all of which have positive α.[4,8,9] Another challenge is a high leakage current density of STO. Hence, Al_2O_3, with its large bandgap of 8.7 eV, is considered a good candidate, because it can reduce the leakage current to less than 10^{-7} A/cm^2.[10] However, this occurs at the expense of the capacitance density, owing to a smaller κ value of A_2O_3, ~ 10. Currently, ZrO_2 is used in DRAM capacitors, but it is generally accepted that reduction of the current density with the $Al_2O_3/ZrO_2/Al_2O_3$ nano-laminate for sub-20 nm technology is unrealistic.[11] To achieve a larger capacitance density, high-κ materials such as TiO_2, with positive α, are better candidates. A capacitance density of ~100 fF/um^2 has been reported for a (0.5 nm)TiO_2/(7 nm)STO bilayer; however, the current density was above 10^{-7} A/cm^2 at 1 V, owing to the smaller bandgap of TiO_2, of ~3 eV.[12,13] Therefore, different types of TiO_2/STO structures must be produced and the fabrication conditions must be optimized.

In this study, a MIM structure with a TiO_2 thin layer sandwiched between two STOs (STO/TiO_2/STO) was designed and prepared using RF and DC magnetron plasma sputtering. The thickness of the TiO_2 layer was varied while those of the STO layers were kept constant. The top and bottom TiN electrodes were used to avoid the formation of interfaces between TiN and STO.[10] The SiO_2 film was deposited to minimise the leakage current by increasing the resistivity of the substrate. All the oxide films were deposited in oxygen-rich plasma by controlling the flow of oxygen to decrease the effects of the defects generated by oxygen vacancies. The variations in the capacitance density and current density were measured to determine the electrical properties, and XRD and Raman scattering analyses were performed to examine the film morphology.

2. Experimental details

An AJA ATC Orion system equipped with five magnetrons equipped with RF (13.56 MHz) and DC power supply

*Project supported by the City University of Hong Kong Applied Research Grant (ARG) of China (Grant No. 9667122). One of the authors, Mr. Saqib Jabbar, is grateful to the Higher Education Commission (HEC) of Pakistan for financial support under IRSIP.

†Corresponding author. E-mail: saqib.jabbar@gcu.edu.pk

© 2017 Chinese Physical Society and IOP Publishing Ltd

at the City University of Hong Kong was used for depositing TiN/STO/TiO_2/STO/TiN/SiO_2/Si thin films. P-type Si (100) 1×1 cm^2 samples were used as substrates. The samples were cleaned in an ultrasonic bath with acetone, methanol, and deionized water sequentially, for 15 min each. The oxide films were deposited on an RF magnetron system using 99.99% pure SiO_2, STO, and titanium (Ti) targets. Oxygen was also supplied using argon (Ar) as the sputtering gas during deposition, for minimising defects induced by oxygen deficiencies. The TiN films were deposited using DC magnetron sputtering and the optimal deposition conditions were determined by measuring the film thickness using a MCM-160 rate/thickness meter with the shutter closed. The sample holder was rotated at 50 rev/min at a fixed distance of 10 cm. The vacuum chamber was evacuated to a base pressure of 1×10^{-7} Torr with the shutter open and the films were deposited at room temperature. The deposition rate was 0.3 Å/s and the deposition time was increased in steps of 3 min. The approximate thicknesses, T_1, T_2, T_3, T_4, and T_5 of TiO_2, were 5.4 nm, 10.8 nm, 16.2 nm, 21.6 nm, and 27 nm, respectively. Finally, the TiN top electrodes were sputter-deposited using a mask containing 7.8×10^{-3} mm^2 holes. The important deposition parameters are listed in Table 1.

Table 1. Important experimental parameters.

Thin film	Ar flow/sccm	O_2 flow/sccm	N_2 flow/sccm	Power/W	Pressure/mTorr	Deposition rate/Å·s^{-1}	Time/min
SiO_2	15	3	-	200	2.3	0.9	19
STO	15	5	-	200	2.7	0.9	19
TiO_2	15	5	-	200	1.8	0.3	3
TiN	5	-	15	130	1.8	0.8	40

3. Results and discussion

Figure 1(a) shows the XRD patterns of the deposited films. No peaks are associated with SiO_2, indicating that the SiO_2 thin film is amorphous. After the deposition of TiN on the SiO_2/Si substrate, a mixed-structure TiN film with the (111) preferred orientation (JCPDS 38-1420)[14] was observed. The sharp peak observed for the STO thin film on TiN/SiO_2/Si was attributed to the perovskite structure of STO.[15]

Pure perovskites have the cubic structure with poor porosity and small specific surface area. Surfaces are more suitable for avoiding intermixture of particles from the TiO_2 and STO films owing to adsorption, diffusion, and surface reactions. TiN was chosen as the electrode material because it has been reported that TiN films prevent the diffusion of STO and TiN films[10] and are more suitable than TaN electrodes. By depositing TiO_2 films on STO/TiN/SiO_2/Si substrates, we obtained crystalline films with the predominant anatese-TiO_2 phase, also demonstrating the presence of the rutile phase. The anatese phase has been reported to exhibit comparatively smaller κ-values, in the 30–70 range,[16] compared with the rutile phase, for which the κ-value is ~110. The rutile phase has been reported to form for $T > 700$ °C, potentially affecting the thermal budget of the process. It has been reported that by controlling the DC or RF magnetron sputtering conditions, the rutile phase can be obtained without heat treatment.[17–19] In Fig. 1(b), a FE-SEM micrograph of the film with a thickness of T_2 reveals a stacked structure of the film. Although the thickness of the TiO_2 film could not be accurately measured owing to the fact that a diamond cutter eventually damages the structure, the thickness of the STO layer was estimated to be ~100 nm, which is close to the expected thickness determined by a thickness meter. No interface was observed at the film boundaries, and the film thickness was uniform.

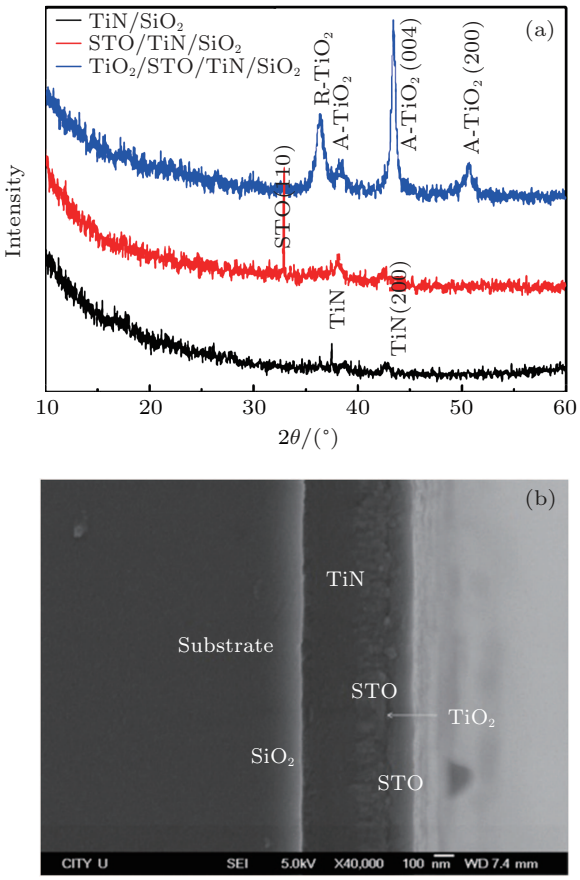


Fig. 1. (color online) (a) XRD patterns of the different stacked structures on Si (100), and (b) a FE-SEM micrograph of the sandwiched TiO_2 film with a thickness of T_2.

Figure 2 shows the Raman scattering spectra of the structure, before and after the deposition of the last STO film on

TiO_2. The spectra were obtained using a Renishaw Raman System 2000 equipped with a 514 nm Ar laser. Although the TiO_2 film is very thin (∼5.4 nm), prominent peaks associated with anatese TiO_2 are observed at 147.7 cm^{-1} and 630 cm^{-1}.[20] No peaks associated with the rutile phase are observed, confirming that the dominant phase is anatese. Owing to the small thickness of the TiO_2 film, the spectrum also includes contributions of reflections from the STO films. The obtained spectrum was compared to previously reported spectra for Sr- and Ti-rich or deficient STO films, and based on this comparison the deposited films were preferentially stoichiometric. The second-order peaks at 218 cm^{-1} and 303 cm^{-1} reveal the presence of the stoichiometric STO films similar to the XRD results, while the small hump at 350 cm^{-1} may arise from the Sr-rich STO.[21,22] The small-intensity broad peak at ∼535 cm^{-1} indicates the first-order Raman process. The intensity depends on the film thickness and it increased for thicknesses $>$ 1000 nm. Better crystallinity was observed for the thinner films than the thicker ones.[23] Although the intensity of the first-order peak is very small, it reveals the presence of crystal defects, which may be owing to the deficiency of oxygen atoms inducing a strain in the films.[20,21,23] This is because oxygen deficiency in TiO_2 films yields structural defects. After the deposition of the STO films on TiO_2, the intensity of the peaks associated with TiO_2 diminished, and the STO peaks became narrower. The broad spectral features in the 550–800 cm^{-1} indicate that the STO film is not a single crystal.[23]

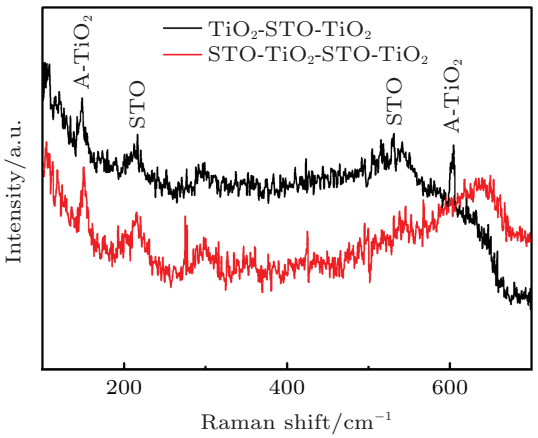


Fig. 2. (color online) Raman spectra of different structures on the TiN/SiO_2/Si substrate.

The *I–V* and *C–V* characteristics were determined using a Keithley 4200 SCS system at 1 MHz and 25 mV AC. Figure 3(a) shows how the *I–V* curves of the capacitors change as the TiO_2 film thickness changes from T_1 to T_5. For T_1, the leakage current is sufficiently high, $\sim 1.5 \times 10^{-6}$ A at 1 V, and it abruptly increases above ±2.1 V. It can be assumed that the TiO_2 film with such a small thickness compared to the bulk material acts as an interface and controls the leakage current

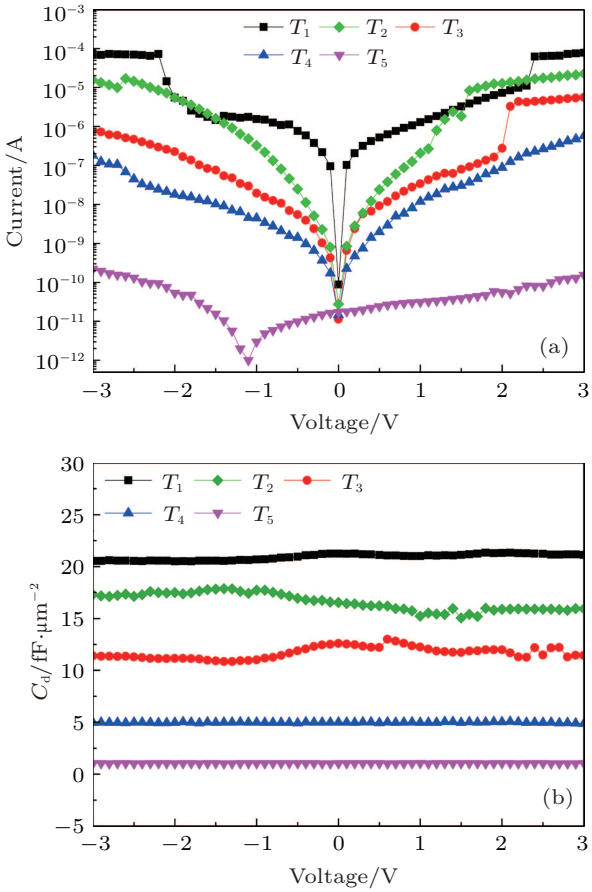


Fig. 3. (color online) (a) *I–V* characteristics and (b) CV characteristics of devices with different TiO_2 thicknesses.

of the capacitor. In this case, the bulk material is assumed highly conductive, owing to a large concentration of defects (oxygen vacancies or other structural defects). The abrupt increase in the current at 2.3 V suggests that trap states are generated below the conduction band. It has been proposed that if the interface plays a dominant role, then the leakage current should be attributed to the Schottky emission (SE), but if the bulk plays the dominant role, the leakage current should be attributed to the Poole–Frenkel emission (PFE).[24] With regard to T_1, at a small positive voltage ($V < 2.3$ V), the current increases linearly, exhibiting ohmic behavior. As the voltage increases, the electric field across the dielectric becomes sufficiently strong for injecting electrons into the near-interfacial states, subsequently sharply increasing the leakage current, as shown in the figure. These states are created owing to a positive potential generated by the presence of structural or oxygen vacancy defects. With regard to T_2, the leakage current drops to 2×10^{-7} A, but the interface still appears to play a dominant role in controlling the leakage current, because the current is still very large. There is a small increase in the current at 1.5 V, exhibiting the same behaviour as that observed for T_1. The increase in the slope of the leakage current for V in the 0–1.5 V range, and the small increase in the current indicate that the decrease in the positive potential is owing to defects. This means that by further increasing the thickness of TiO_2, the defects

are alleviated, correspondingly decreasing the positive potential. For T_3, it is difficult to determine whether the interface or the bulk is dominant. The *I*–*V* curves exhibit the same behaviour as for T_1 and T_2, with a reduced leakage current of 3.5×10^{-8} A at 1 V, in addition to the abrupt current increase at 2 V, signalling the reappearance of defects. The smaller positive potential than that for T_1 indicates that there are fewer defects for T_3. By increasing the thickness to T_4, the leakage current decreases further to 1.3×10^{-8} A, and the curve does not change as sharply as before. The almost symmetrical and smooth shape of the curve around 0 V indicates that the leakage current is dominated by the bulk and the mechanism is PFE, SE, or both. For the thickness T_5, the current decreases to 3.3×10^{-11} A at 1 V and the curve is asymmetrical around 0 V. The minimum of the curve at the negative voltage is owing to the migration of defects through the bulk, which creates positive fixed charges under the electrode area.[25]

Figure 3(b) shows how the capacitance density (C_d) depends on the applied voltage, for different thicknesses. In all cases, the dependencies are almost straight lines, which is owing to the combined effect of α of STO and TiO_2. The capacitance density is given by $C_d = A\varepsilon_d/(1.6\times10^{-19}T)$, where ε_d is the permittivity of the dielectric material (F/cm), A is the area of the capacitor, and T is the overall effective thickness of the insulator (STO + TiO_2 + STO); thus, C_d is inversely proportional to the effective thickness of the insulator.[26] Figure 3(b) is consistent with previous results, according to which C_d decreases with increasing TiO_2 thickness.[9,27] For T_1, C_d attains a maximal value of $\sim$20 fF/um^2 and the curve is nearly a straight line. The smooth variations in the capacitance at 0 V and 1.8 V indicate a uniform concentration of defects under the electrode. By increasing the thickness to T_2, C_d decreases to $\sim$16 fF/um^2, with small fluctuations owing to the motion of positively charged defects. The CV curve of T_3 is similar to that of T_1, showing variations at 0 V and 1.85 V, but it is not smooth, indicating a non-uniform concentration of defects under the electrode, with C_d decreasing to 11 fF/um^2 for T_3. With regard to T_4 and T_5, the CV curves are straight owing to the bulk effect of the capacitor, as explained before when discussing the *I*–*V* characteristics. The C_d values are 5 fF/um^2 and 1 fF/um^2 for T_3 and T_4, respectively, and the leakage current is inversely related to C_d.

4. Conclusion

The effects of a sandwich TiO_2 layer on the electrical properties of STO were investigated by varying the TiO_2 layer's thickness. XRD and Raman scattering analyses suggest that the deposited films are crystalline and the predominant phase is anastase. The capacitance density varies almost linearly with the applied voltage and the fluctuations in the CV curves decrease with increasing thickness. Maximum capacitance density is obtained for the smallest thickness ($\sim$5.4 nm) and it decreases as the film becomes thicker. The leakage current also decreases with thickness but it is still quite high. Additional research is needed for optimising the conditions required for reducing the leakage current, while retaining a high capacitance.

References

[1] Kaynak C B, Lukosius M, Costina I, Tillak B, Wenger Ch, Ruhl G and Blomberg T 2011 *Thin Solid Films* **519** 5734

[2] Pontes F M, Leite E R, Lee E J H, Longo E and Varela J A 2001 *J. European Ceramic Society* **21** 419

[3] Maletic S, Maletic D, Petronijevic I, Dojcilovic J and Popovic D M 2014 *Chin. Phys. B* **23** 26102

[4] Jorel C, Vallee C, Gonon P, Gourvest E, Dubarry C and Defay E 2009 *Appl. Phys. Lett.* **94** 253502

[5] Kahn M, Vallee C, Defay E, Dubourdieu C, Bonvalot M, Blonkowski S, Plaussu J R, Garrec P and Baron T 2007 *Microelectron. Reliab.* **47** 773

[6] Durand C, Vallee C, Dubourdieu C, Kahn M, Derivaz M, Blonkowski S, Jalabert D, Hollinger P, Fang Q and Boyd I W 2006 *J. Vac. Sci. Technol. A* **24** 459

[7] Kim S J, Cho B J, Li M F, Ding S J, Zhu C, Yu M B, Narayanan B, Chin A and Kwong D L 2004 *IEEE Electron Device Lett.* **25** 538

[8] Park S D, Park C, Gilmer D C, Park H K, Kang C Y, Lim K Y, Burham C, Barnett J, Kirsch P D, Tseng H H, Jammy R and Yeom G Y 2009 *Appl. Phys. Lett.* **95** 022905

[9] Park I S, Ryu K, Jeong J and Ahn J 2013 *IEEE Electron Device Lett.* **34** 120

[10] Kaynak C B, Lukosius M, Tillack B, Wenger Ch, Blomberg T and Ruhl G 2011 *Microelectronic Engineering* **88** 1521

[11] Martin D, Grube M, Weinreich W, Muller J, Weber W M, Schroder U, Reichert H, and Mickolajick T 2013 *J. Appl. Phys.* **113** 194103

[12] Popovici M I, Swerts J, Kessel-lo,Pawlak M, Kim M S, Kittl J and Elshocht S V (U. S. Patent) 0092807 A1 [2012-04-19]

[13] Popovici M I, Swerts J, Redolfi A, Kaczer B, Aoulaiche M, Radu I, Clima S, Everaert J L, Elshocht S V and Jurczak M 2014 *Appl. Phys. Lett.* **104** 082908

[14] Chen H Y and Lu F H 2005 *J. Vac. Sci. Technol. A* **23** 1006

[15] Demirors A F and Imhof A 2009 *Chem. Mater.* **21** 3002

[16] Stamate M D 2003 *Appl. Surf. Sci.* **218** 317

[17] Sima C, Waldhauser W, Lackner J, Kahn M, Nicolae I, Viespe C, Grigoriu C and Manea A 2007 *J. Optoelectronics Adv. Mater.* **9** 1146

[18] Sicha J, Herman D, Musil J, Stryhal Z and Pavlik J 2007 *Plasma Process. Polym.* **4** S345

[19] Okimura K, Shibata A, Maeda N, Tachibana K, Noguchi Y and Tsuchida K 1995 *Jpn. J. Appl. Phys.* **34** 4950

[20] Park S J, Lee J P, Jang J S, Rhu H, Yu H, You B Y, Kim C S, Kim K J, Cho Y J, Baik S and Lee W 2013 **24** 295202

[21] Tenne D A, Farrar A K, Brooks C M, Heeg T, Schubert J, Jang H W, Bark C W, Folkman C M, Eom C B and Schlom D G 2010 *Appl. Phys. Lett.* **97** 142901

[22] Rabuffetti F A, Kim H S, Enterkin J A, Wang Y, Lanier C H, Marks L D, Peoppelmeier K R and Stair P C 2008 *Chem. Mater.* **20** 5628

[23] Murkulov V I, Fox J R, Li H C, Si W, Sirenko A A and Xi X X 1998 *Appl. Phys. Lett.* **72** 3291

[24] Scott J F 2006 *J. Phys. Cond. Matt.* **18** R361

[25] Mojarad S A, Kwa K S K, Goss J P, Zhou Z, Ponon N K, Appleby D J R, Al-Hamadany R A S and O'Neill A 2012 *J. Appl. Phys.* **111** 014503

[26] Borja J P, Lu T M and Plawsky J 2016 *Dielectric Breakdown in Gigascale Electronics: Time dependent Failure Mechanisms* (Springer) p. 32

[27] Wang C and Kim N Y 2009 *Trans. Electr. Electron Mater.* **10** 147